

## CONTRASTING PATHWAYS TO MOTT GAP COLLAPSE IN ELECTRON AND HOLE DOPED CUPRATES

R. S. MARKIEWICZ

*Northeastern University, 360 Huntington Avenue, Boston MA 02115, USA*  
*E-mail: markiewic@neu.edu*

Recent ARPES measurements on the electron-doped cuprate  $\text{Nd}_{2-x}\text{Ce}_x\text{CuO}_4$  can be interpreted in a mean field model of uniform doping of an antiferromagnet, with the Mott gap closing near optimal doping. Mode coupling calculations confirm the mean field results, while clarifying the relation between the Mott gap and short-range magnetic order. The *same* calculations find that hole doped cuprates should follow a strikingly different doping dependence, involving instability toward spiral phases or stripes. Nevertheless, the magnetic order (now associated with stripes) again collapses near optimal doping.

### 1. Introduction

#### 1.1. Mode Coupling Theories

In conventional itinerant ferro- and antiferromagnets, mode-coupling theories<sup>1,2</sup> have proven of value in treating the role of fluctuations in reducing or eliminating long-range order, as well as in the development of local moments, Curie-like susceptibility, and in general the crossover to magnetic insulators. Similar approaches have been applied to charge-density wave systems<sup>3</sup> and the glass transition<sup>4</sup>.

Attempts to apply such a formalism to study the antiferromagnetism of the cuprate superconducting compounds have been frustrated, since the antiferromagnetic (AF) phase is found to be unstable against hole doping, toward either an incommensurate AF phase<sup>5</sup> or phase separation<sup>6</sup>. Here, it is demonstrated that this tendency to instability is either absent or greatly reduced in electron-doped cuprates, and the mode coupling analysis can provide a detailed description of the collapse of the Mott gap with doping. The results are of great interest of themselves: the collapse is associated with one or more quantum critical points (QCPs), and superconductivity is optimized close to one QCP. However, the results have an additional importance in the light they shed on the more complicated problem of the *hole doped* cuprates. First, the effective Hubbard  $U$  parameter has a

significant doping dependence, from  $U \sim W$  at half filling (where  $W = 8t$  is the bandwidth and  $t$  the nearest neighbor hopping parameter) to  $U \sim W/2$  near optimal doping. Secondly, the *same* mode coupling theory which works so well for electron-doped cuprates, *breaks down* for hole doping, due to the above noted electronic instability. This suggests that (a) the electron-hole asymmetry must be due to a band structure effect and (b) a suitable generalization of mode coupling theory should be able to incorporate the effects of this instability.

## 1.2. ARPES of $\text{Nd}_{2-x}\text{Ce}_x\text{CuO}_4$

Recently, Armitage, et al.<sup>7</sup> succeeded in measuring angle-resolved photoemission spectra (ARPES) of  $\text{Nd}_{2-x}\text{Ce}_x\text{CuO}_4$  (NCCO) as a function of electron doping, from essentially the undoped insulator  $x = 0$  to optimal doping  $x = -0.15$ . The doping dependence is strikingly different from that found in *hole-doped*  $\text{La}_{2-x}\text{Sr}_x\text{CuO}_4$  (LSCO)<sup>8,9</sup>. Both systems start from a Mott insulator at half filling, with ARPES being sensitive only to the lower Hubbard band (LHB), approximately 1eV below the Fermi level  $E_F$ . With hole doping, the LHB remains well below  $E_F$  while holes are added in mid-gap states (as expected, e.g., in the presence of nanoscale phase separation<sup>10</sup>); for electron doping, the Fermi level shifts to the upper Hubbard band (UHB), and the electrons appear to uniformly dope the antiferromagnet.

Remarkably, the full doping dependence can be simply described by a mean-field (MF)  $t-t'-U$  Hubbard model<sup>11</sup>, where  $t'$  is the second neighbor hopping,  $U$  is the onsite coulomb repulsion, and a one band (copper only) model was assumed for simplicity.<sup>a</sup> A key finding is that the Hubbard  $U$  is doping dependent, leading to a quantum critical point (QCP) just beyond optimal doping, where the Mott gap vanishes. The appearance of a peak in superconductivity near an AFM QCP is a fairly common occurrence<sup>12</sup>; in particular, something similar has been observed<sup>13</sup> in the hole-doped cuprates. However, the MF theory is problematic, in that the Mott gap is associated with long-range Néel order, and the MF model predicts anomalously high values for  $T_N$ .

---

<sup>a</sup>Actually, in Ref. <sup>11</sup> a third neighbor hopping  $t''$  was included to optimize the fit to the experimental Fermi surface curvature. The changes induced by this parameter are small, and it will be ignored in the present calculations.

## 2. Mode Coupling Theory

This anomalous behavior can be cured by incorporating the role of fluctuations. Indeed, it is known that in a two-dimensional system, the Néel transition can only occur at  $T = 0$  – the Mermin-Wagner (MW) theorem<sup>14</sup>. By treating fluctuations within a mode coupling analysis, the MW theorem is satisfied<sup>15</sup>, and the Mott gap is completely decoupled from long-range spin-density wave (SDW) order. Even though  $T_N = 0$  a large Mott (pseudo)gap is present even well above room temperature near half filling – due to *short-range* AFM order. The MF gap and transition temperature are found to be approximately the pseudogap and  $T^*$  the onset temperature for the pseudogap opening.

The calculation can be summarized as follows. In a path integral formulation of the Hubbard model<sup>16</sup>, the quartic term is decoupled via a Hubbard-Stratonovich transformation and the fermionic degrees integrated out. The resulting action is then expanded to quartic order in the Hubbard-Stratonovich fields  $\phi$ . The quadratic interaction reproduces the RPA theory of the Hubbard model – the quadratic coefficient is just  $U\delta_{0q}$ , where  $\delta_{0q}$  is the (inverse) Stoner factor  $\delta_q = 1 - U\chi_0(\vec{Q} + \vec{q}, \omega)$  (here  $\vec{Q} = (\pi, \pi)$  is the wave vector associated with the commensurate SDW). The quartic interaction, parametrized by the coefficient  $u$  evaluated at  $\vec{Q}$ ,  $\omega = 0$ , represents coupling between different magnetic modes. The effects of this term cannot be treated in perturbation theory, and a self-consistent renormalization (SCR) scheme<sup>2</sup> is introduced to calculate the renormalized Stoner factor  $\delta_q = \delta_{0q} + \lambda$ . A self-consistent equation for  $\delta$  is found, which can be solved if the band parameters and the interactions  $U$  and  $u$  are known.

To simplify the calculation,  $\lambda$  is assumed to be independent of  $\vec{q}$  and  $\omega$ , and the Stoner factor is expanded near  $\vec{Q}$  as

$$\delta_q(\omega) = \delta + Aq^2 - B\omega^2 - iC\omega, \quad (1)$$

similar to the form assumed in nearly antiferromagnetic Fermi liquid (NAFL)<sup>17</sup> theory. The imaginary term linear in frequency is due to the presence of low energy magnon excitations in the vicinity of the ‘hot spots’ – the points where the Fermi surface intersects the Brillouin zone diagonal. Here fluctuations toward long-range Néel order lead to strong, Bragg-like scattering which ultimately leads to the magnetic Brillouin zone boundary at  $T_N$ . Independent of the parameter values, it is found that  $\delta > 0$  for  $T > 0$  – the MW theorem is satisfied, while for electron doping  $\delta \rightarrow 0$  as  $T \rightarrow 0$  up to a critical doping – there is a QCP associated with  $T = 0$  SDW order. For hole doping the calculation breaks down – the parameter  $A$  is negative in a significant doping regime, as will be discussed further below.

The key insights of mode coupling theory are:

- The Mott transition is dominated by hot spot physics, which creates zone-edge magnons. The condensation of these magnons creates a new zone boundary, and opens up a gap (the Mott gap) in the electronic spectrum. In two dimensions (2D), there can be no Bose condensation at finite temperatures, but the pileup of lowest energy magnons as  $T$  decreases leads to the appearance of a Mott pseudogap and a  $T=0$  transition to long-range SDW order.

- Evidence for the existence of local magnons comes from well-defined *plateaus* in the spin susceptibility. Plateaus are seen in (a) the doping dependence of the susceptibility at  $\vec{Q}$ , (b) the  $\vec{q}$  dependence of the susceptibility near  $\vec{Q}$ , and (c) the  $\omega$  dependence of the susceptibility (both real and imaginary parts) at  $\vec{Q}$ . These plateaus introduce *cutoffs* in the  $\vec{q}$  and  $\omega$  dependence of the Stoner factor, Eq. 1, which in general *cannot* be sent to  $\infty$ , in contrast to the NAFL model. Also, the flatness of the plateau tops makes it difficult to estimate the model parameters from first principles. In particular  $A$  is strongly temperature dependent, while  $u$  is anomalously small (this problem had been noted previously<sup>18</sup>).

- A finite Néel temperature can be generated by interlayer coupling. In the cuprates, such coupling is typically frustrated, and Néel order more likely arises from a Kosterlitz-Thouless transition, after the spin dimensionality is reduced by, e.g., spin-orbit coupling<sup>19</sup>.

### 3. Results

#### 3.1. Susceptibility

In analyzing the ARPES data, a tight-binding band is assumed,

$$\epsilon_k = -2t(c_x + c_y) - 4t'c_x c_y, \quad (2)$$

with  $c_i = \cos k_i a$ ,  $t = 0.326eV$ , and  $t'/t = -0.276$ . The Hubbard  $U$  is doping dependent,  $U/t = 6, 5, 3.5$ , and  $2.9$  at  $x = 0, -0.04, -0.10$ , and  $-0.15$ , respectively, and the mode coupling constant is adjusted to reproduce the low-temperature spin stiffness at half filling<sup>20</sup>,  $u^{-1} = 0.256eV$ . The bare susceptibility

$$\chi_0(\vec{q}, \omega) = - \sum_{\vec{k}} \frac{f(\epsilon_{\vec{k}}) - f(\epsilon_{\vec{k}+\vec{q}})}{\epsilon_{\vec{k}} - \epsilon_{\vec{k}+\vec{q}} + \omega + i\delta}, \quad (3)$$

is evaluated near  $\vec{Q}$  to determine the parameters of Eq. 1.

The susceptibility  $\chi_0(\vec{Q}, 0)$  has approximately the shape of a plateau as a function of doping, Figure 1a, bounded by the critical points  $x_H$  and  $x_C$

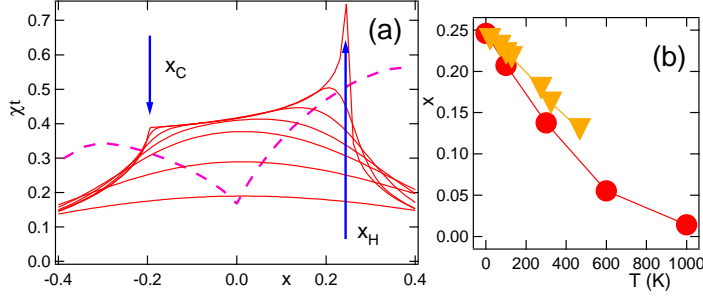


Figure 1. (a) Susceptibility  $\chi_0$  at  $\vec{Q}$  as a function of doping for several temperatures. From highest to lowest curves near  $x = 0.1$ , the temperatures are  $T = 1, 100, 300, 600, 1000, 2000,$  and  $4000$  K. Dashed line =  $1/U_{eff}$ . (b) Circles = pseudo-VHS (peak of  $\chi_0$ ) as a function of temperature  $T_V$ ; triangles =  $T_{incomm}$ .

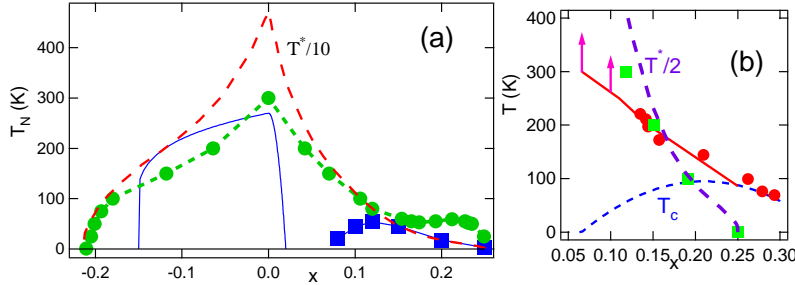


Figure 2. (a) Mean-field transition temperature  $T^*$  (long dashed line) compared with Néel temperature of NCCO and LSCO (solid line) plus magnetic transition temperature of stripe ordered phase in Nd-substituted LSCO<sup>25</sup>, Circles = model calculation of  $T_N$  assuming unfrustrated interlayer hopping. (b) Comparison of mean-field transition (long dashed line) to various estimates of pseudogap temperature: from photoemission<sup>22</sup> (solid line), heat capacity<sup>23</sup> (squares) and tunneling<sup>24</sup> (circles =  $\Delta/3$ , with  $\Delta$  the tunneling gap). Short dashed line = superconducting  $T_c$ .

where the Fermi surface ceases to have hot spots. These special points act as *natural phase boundaries* for antiferromagnetism, due to the sharp falloff in  $\chi$  off of the plateau.

The special point  $x_H$  coincides at  $T = 0$  with the Van Hove singularity (VHS) of the band. Remarkably, the susceptibility peak has a strong temperature dependence<sup>21</sup>, defining a pseudo-VHS; Fig. 1b shows the temperature  $T_V(x)$ , at which the susceptibility peaks at  $x$ . This can be understood by noting that the energy denominator of  $\chi$ , Eq. 3, is *independent of  $t'$* , and thus would lead to a large peak at half filling,  $x=0$  (associated with states along the zone diagonal). At low temperatures, the difference in Fermi functions in the numerator cuts this off, and forces the peak to coincide

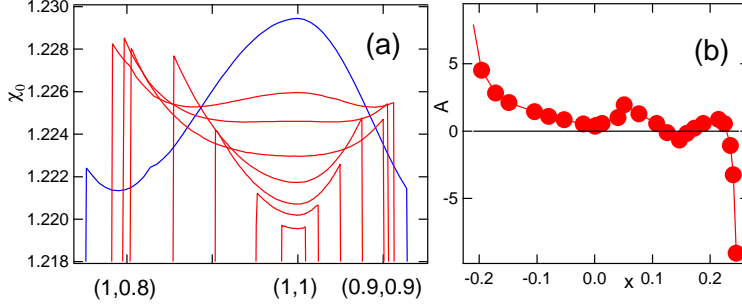


Figure 3. (a) Expanded view of susceptibility  $\chi_0$  on the plateaus near  $\vec{Q}$  for a variety of dopings at  $T = 1K$ . From highest to lowest curves near  $\vec{Q}$ , the chemical potentials are  $\mu = -0.25, -0.22, -0.21, -0.20$  ( $x=0$ ),  $-0.15, -0.10, -0.05$ , and  $-0.02eV$ . All curves except  $\mu = -0.20eV$  have been shifted vertically to fit within the expanded frame. (b) Calculated  $A(x)$ .

with the VHS. As  $T$  increases, more states near the zone diagonals become available, causing the peak susceptibility to shift towards half filling. For a temperature  $T_{incomm}$  slightly above  $T_V$ , the curvature  $A$  becomes negative, signalling the instability of the commensurate AFM state.

The dashed line in Fig. 1a represents  $1/U_{eff}$ , where  $U_{eff}$  is a doping dependent Hubbard  $U$ , estimated from a screening calculation<sup>11</sup>. The intersection of the dashed line with one of the solid lines defines the mean-field Néel transition,  $\chi_0 U_{eff} = 1$ , Fig. 2a (long-dashed line). As will be shown below, once fluctuations are included, the mean field transition turns into a pseudogap onset  $T^*$ , while the actual onset of long range magnetic order is suppressed to much lower temperatures. From Fig. 2b, it can be seen that the mean-field  $T^*$  is consistent with a number of estimates<sup>22,23,24</sup> of the experimental pseudogap for *hole* doping, while a simple calculation of the three-dimensional Néel transition associated with interlayer coupling (circles in Fig. 2a – see the Appendix for details) can approximately reproduce the experimental observations (solid lines) – if the transitions associated with magnetic order on quasistatic stripes<sup>25</sup> are included (squares).

In addition to plateaus in *doping*, the hot spots lead to plateaus in the frequency and wave number dependence of  $\chi_0(\vec{q}, \omega)$ . For instance, Fig. 3a shows plateaus in  $\chi_0(\vec{Q} + \vec{q}, 0)$  at a series of dopings at  $T = 1K$ . Once  $\chi_0$  is known the parameters  $A$  and  $C$  of Eq. 1 can be calculated;  $B$  is quite small, and can in general be neglected. The plateau width  $q_c \rightarrow 0$  as  $x \rightarrow x_C$ , leading to a strong  $T$ -dependence of  $A$ , Fig. 3b.

+

Given the model parameters, the self-consistent equation for  $\delta$  becomes<sup>15</sup>

$$\delta = \delta_0 + \frac{3ua^2}{\pi^2 C} \int_0^{q_c} dq'^2 \int_0^{\alpha_\omega} dx \coth\left(\frac{x}{2CT}\right) \frac{x}{(\delta + Aq'^2)^2 + x^2}. \quad (4)$$

which has the approximate solution

$$Z\delta - \bar{\delta}_0 = \frac{3ua^2 T}{\pi A} \ln\left(\frac{2CT}{e\delta}\right), \quad (5)$$

where  $\bar{\delta}_0 = \delta_0 + \eta - 1$ ,

$$\eta = 1 + \frac{3uq_c^2 a^2}{\pi^2 C} \left( \frac{1}{2} \ln[1 + a_q^{-2}] + \frac{\tan^{-1}(a_q)}{a_q} \right), \quad (6)$$

$a_q = Aq_c^2/\alpha_\omega$ , and  $q_c$  and  $\alpha_\omega$  are wavenumber and (normalized) frequency cutoffs, respectively, and the exact form of  $Z$  is not required. From the logarithm in Eq. 5,  $\delta$  must be greater than zero for all  $T > 0$ , so there is no finite temperature phase transition. At low temperatures, the  $\delta$  on the left hand side of Eq. 5 can be neglected, leading to a correlation length

$$\xi^2 = \frac{A}{\delta} = \xi_0^2 e^{4\pi\rho_s/T}, \quad (7)$$

with  $\xi_0^2 = eA/2TC$  and

$$\rho_s = \frac{\pi A |\bar{\delta}_0|}{24ua^2}. \quad (8)$$

Here,  $\bar{\delta}_0$  is the quantum corrected Stoner factor, *which controls the  $T = 0$  QCP*: there is long-range Néel order at  $T = 0$  whenever  $\bar{\delta}_0 \leq 0$ , or  $U\chi_0 \geq \eta$ .

### 3.2. ARPES Data

From the susceptibility, the contribution to the electronic self energy due to one magnon scattering can be calculated. The imaginary part of the susceptibility can be written

$$\begin{aligned} \text{Im}\Sigma(\vec{k}, \omega) &= \frac{-g^2\chi_0}{V} \sum_{\vec{q}} \int_{-\alpha_\omega/C}^{\alpha_\omega/C} d\epsilon [n(\epsilon) + f(\xi_{\vec{k}+\vec{q}})] \times \\ &\quad \times \delta(\omega + \epsilon - \xi_{\vec{k}+\vec{q}}) \frac{C\epsilon}{(\delta + Aq'^2)^2 + (C\epsilon)^2}. \end{aligned} \quad (9)$$

where the coupling is approximately  $g^2\chi_0 \simeq 3U/2$ . Since  $\epsilon$  is peaked near zero when  $\vec{q} \simeq \vec{Q}$ ,  $\text{Im}\Sigma$  is approximately a  $\delta$ -function at  $\xi_{\vec{k}+\vec{Q}}$ . Approximating  $\text{Im}\Sigma = -\pi\bar{\Delta}^2\delta(\omega - \xi_{\vec{k}+\vec{Q}})$ , then

$$\bar{\Delta}^2 = \frac{U}{8u} (\delta - \delta_0). \quad (10)$$

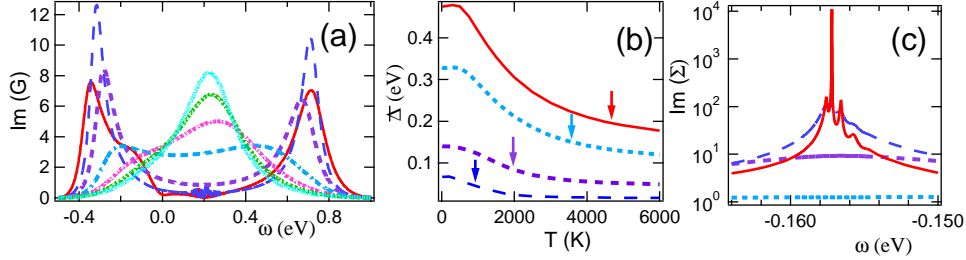


Figure 4. (a) Spectral function for  $x = 0.0$ ,  $\vec{k} = (\pi/2, \pi/2)$ , at  $T = 100, 500, 1000, 2000, 3000, 4000$ , and  $5000$  K (larger splittings corresponding to lower  $T$ 's). (b)  $\bar{\Delta}(T)$ ; solid line:  $x = 0.0$ , dotted lines:  $x = -0.04$ , short-dashed lines:  $x = -0.10$ , long-dashed lines:  $x = -0.15$ . (c)  $\text{Im}(\Sigma)$  for  $x = 0$ ,  $\vec{k} = (\pi, 0)$  at  $T = 100$  (solid line),  $500$  (long dashed line),  $1000$  (short dashed line), and  $2000$  K (dotted line).

The importance of this result can be seen by noting that, by Kramers-Kronig,

$$\text{Re}\Sigma(\vec{k}, \omega) = \frac{\bar{\Delta}^2}{\omega - \xi_{\vec{k}+\vec{Q}}}, \quad (11)$$

so that

$$G^{-1}(\vec{k}, \omega) = \omega - \xi_{\vec{k}} - \text{Re}\Sigma^R(\vec{k}, \omega) = \frac{(\omega - \xi_{\vec{k}})(\omega - \xi_{\vec{k}+\vec{Q}}) - \bar{\Delta}^2}{\omega - \xi_{\vec{k}+\vec{Q}}}. \quad (12)$$

The zeroes of  $G^{-1}$  are identical to the mean field results for long-range AFM order<sup>26,11</sup>, except that the long-range gap  $\Delta = U \langle m_z \rangle$  is replaced by the *short-range* gap  $\bar{\Delta} \sim U \sqrt{\langle m_z^2 \rangle}$ .

Figure 4a shows the spectral function  $A(\vec{k}, \omega) = \text{Im}(G(\vec{k}, \omega))/\pi$  for  $x = 0$  at  $\vec{k} = (\pi/2, \pi/2)$  at a series of temperatures. The spectrum is split into upper and lower Hubbard bands, with a gap approximately  $2\bar{\Delta}$ . The short-range order gap  $\bar{\Delta}$  is plotted in Fig. 4b; it is finite for all temperatures, but increases significantly close to the mean-field Néel temperature (arrows). The net dispersion for two dopings,  $x = 0, -0.15$ , is shown in Fig. 5; it is in good agreement with the experimental<sup>7</sup> and mean-field<sup>11</sup> results. The build up of hot spot magnons is reflected in the growth of  $\text{Im}(\Sigma(\vec{k}, \omega))$  near  $\omega = \xi_{\vec{k}+\vec{Q}}$ , Fig. 4c (note the logarithmic scale).

#### 4. Implications for Hole Doping

One expects, and observes, a certain degree of symmetry between electron and hole doping: there is a susceptibility plateau associated with hot spots, Fig. 1, which terminates near optimal doping; the termination of magnetic order in electron-doped cuprates at a QCP near optimal doping is matched



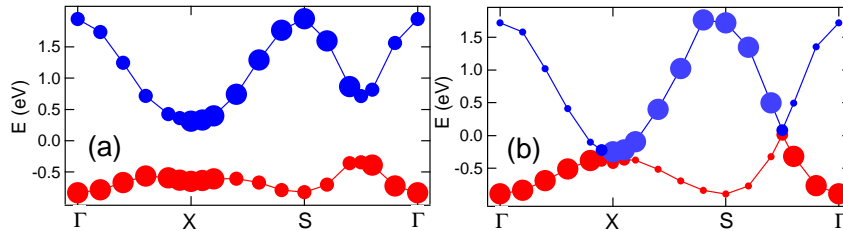


Figure 5. Dispersion relations for (a)  $x=0$  and (b)  $x=-0.15$ , at  $T=100\text{K}$ . Brillouin zone directions are  $\Gamma = (0, 0)$ ,  $X = (\pi, 0)$ ,  $S = (\pi, \pi)$ .

in hole-doped cuprates by the observation of a QCP near optimal doping which appears to be associated with loss of magnetic correlations<sup>13</sup>; and in both cases an optimal, probably d-wave superconductivity is found near the QCP. Also, it is expected that  $U$  would have a similar decrease with doping for either electron or hole doping (see the model calculation, dashed line in Fig. 1).

On the other hand, there are also significant differences, not the least of which is the *magnitude* of the superconducting  $T_c$ . Most significantly, there is considerable evidence for the appearance of nanoscale phase separation – either in the form of stripes<sup>27</sup> or blobs<sup>28</sup> – for hole doped cuprates, while the evidence is weaker or absent for electron doping<sup>29,30</sup>. As noted above, this difference arises naturally within the present calculations, which find instability of the commensurate magnetic order for hole doping only (e.g., Fig. 3).

Given these similarities and differences, the present calculations can shed some light on aspects of hole-doped physics:

(1) A large *pseudogap* is present at half filling, associated with short-range magnetic order. Just as for electron doping, it should persist with hole doping until short-range magnetic order is lost. The observed<sup>13</sup> connection of the loss of magnetic fluctuations with the collapse of the pseudogap near  $x = 0.19$  strongly suggests an identification of the observed pseudogap at  $T^*$  with the Mott pseudogap, as found for electron doping. While a number of theories have proposed that the pseudogap is associated with superconducting fluctuations, these seem to turn on at a temperature lower than  $T^*$ .<sup>31</sup> Remarkably, despite the complications associated with stripes, the mean-field transition temperature is within a factor of two of the observed pseudogap temperatures, Fig. 2b.

(2) The present calculations point to a close connection between the Van Hove singularity (VHS) and the instability of commensurate magnetic order, Fig. 1b. This strongly suggests that the VHS is responsible for the

asymmetry between electron and hole doping, and in particular for any frustrated phase separation.

(3) If the stripes are associated with frustrated phase separation, it is important to identify the second (metallic) phase and understand what interaction stabilizes it (particularly since this is likely to be the phase in which high- $T_c$  superconductivity arises). In a purely Hubbard model, this would be a ferromagnetic phase, hence probably incompatible with superconductivity. However, the reduction of  $U$  with doping found here strengthens the case for a nonmagnetic charge stripe associated with interactions beyond the Hubbard model<sup>32</sup>.

## 5. Discussion: Polaron Limit

In the very low doping limit, isolated charge carriers should form (spin or charge) polaronic states for either sign of doping. The asymmetry between hole and electron doping would then be reflected in interpolaronic interactions being strongly attractive for hole doping. For electron doping, the isolated polarons could be much more easily pinned in the AFM background, leading to the much stronger localization found in NCCO<sup>33</sup>.

## Acknowledgments

This work has been supported in part by the Spanish Secretaria de Estado de Educación y Universidades under contract n<sup>o</sup> SAB2000-0034. The work was carried out while I was on sabbatical at the Instituto de Ciencia de Materiales de Madrid (ICMM) in Madrid, and the Laboratory for Advanced Materials at Stanford. I thank Paco Guinea, Maria Vozmediano, and Z.X. Shen for inviting me, and for numerous discussions.

## Appendix: c-Axis Coupling

A toy model is introduced to study the effect of interlayer coupling on generating a finite Néel transition temperature  $T_N$ . The interlayer hopping is assumed to be a constant  $t_z$  independent of in-plane momentum. While a term of the form  $t_z(c_x - c_y)^2$  would not greatly change the results, in the physical cuprates alternate  $\text{CuO}_2$  planes tend to be *staggered*, which should lead to frustration  $t_z(\vec{Q}) = 0$ , and greatly reduced interlayer coupling. Indeed, in the cuprates it is entirely possible that interlayer coupling is negligible, and that the Néel transition is actually of Kosterlitz-Thouless form, due to reduced spin dimensionality caused by spin-orbit coupling<sup>19</sup>.

Nevertheless, it is instructive to see how constant- $t_z$  interlayer coupling

can generate a finite  $T_N$ . The revised Eq. 5 can be written in the symbolic form

$$Z\delta = \bar{\delta}_0 + \frac{T}{T_0} \ln\left(\frac{D_0}{D + 2\delta}\right), \quad (\text{A.1})$$

where  $T_0 = \pi^2 A/6ua^2$  and  $D_0 = 4CT/e$  are (doping-dependent) constants (Eq. 5 – the extra  $\pi/2$  in  $T_0$  coming from the  $q_z$ -integral) and<sup>34</sup>  $D \propto t_z^2$ . Thus for finite  $t_z$ , there is a non-zero  $T_N$  given by the solution of  $\bar{\delta}_0 + T/T_0^* = 0$ , with  $T_0^* = T_0/\ln(D_0/D)$ . For the calculation in Fig. 2a, a constant  $T_0^* = 1200K$  was assumed, but it is interesting to note that when the correct doping dependence of the parameters is included,  $T_N \rightarrow 0$  as  $A \rightarrow 0$ , suggesting that the much steeper falloff of  $T_N$  with hole doping is related to phase separation.

Equation A.1 can be rewritten using Eq. 8. The Néel transition occurs when

$$J_z[\xi(T_N)/\xi_0(T_N)]^2 = \Gamma T_N, \quad (\text{A.2})$$

with  $J_z/J = (t_z/t)^2$ ,  $\Gamma = 16C/edU$ ,  $d = D/t_z^2$  and  $J = 4t^2/U$ , suggestive of a form of interlayer coupling proposed earlier<sup>35</sup>.

## References

1. K. K. Murata and S. Doniach, Phys. Rev. Lett. **29**, 285 (1972).
2. T. Moriya, “Spin Fluctuations in Electron Magnetism”, (Springer, Berlin, 1985).
3. P.A. Lee, T.M. Rice, and P.W. Anderson, Sol. St. Commun. **14**, 703 (1974); N. Suzuki and K. Motizuki, in ”Structural Phase Transitions in Layered Transition Metal Compounds”, ed. by K. Motizuki (Reidel, Dordrecht, 1986), p. 135; R.S. Markiewicz, Physica C**169**, 63 (1990); S. Andergassen, S. Caprara, C. Di Castro, and M. Grilli, Phys. Rev. Lett. **87**, 056401 (2001).
4. W. Götze, J. Phys.: Cond. Matt **11**, A1 (1999).
5. B.I. Shraiman and E.D. Siggia, Phys. Rev. Lett. **62**, 1564 (1989).
6. C. Zhou and H.J. Schulz, Phys. Rev. B**52**, 11557 (1995).
7. N.P. Armitage, D.H. Lu, C. Kim, A. Damascelli, K.M. Shen, F. Ronning, D.L. Feng, H. Eisaki, Z.-X. Shen, P.K. Mang, N. Kaneko, M. Greven, Y. Onose, Y. Taguchi, and Y. Tokura, cond-mat/0201119.
8. X.J. Zhou, P. Bogdanov, S.A. Kellar, T. Noda, H. Eisaki, S. Uchida, Z. Hussain, and Z.-X. Shen, Science **286**, 268 (1999).
9. A. Ino, C. Kim, M. Nakamura, T. Yoshida, T. Mizokawa, A. Fujimori, Z.-X. Shen, T. Kakeshita, H. Eisaki, and S. Uchida, Phys. Rev. B **65**, 094504 (2002).
10. R.S. Markiewicz, Phys. Rev. B**62**, 1252 (2000).
11. C. Kusko, R.S. Markiewicz, M. Lindroos, and A. Bansil, cond-mat/0201117.
12. N.D. Mathur, *et al.*, Nature **394**, 39 (1998).

13. J.L. Tallon, J.W. Loram, G.V.M. Williams, J.R. Cooper, I.R. Fisher, J.D. Johnson, M.P. Staines, and C. Bernhard, *Phys. Stat. Sol.* **b215**, 531 (1999).
14. N. D. Mermin and H. Wagner, *Phys. Rev. Lett.* **17**, 1133 (1966).
15. R.S. Markiewicz, unpublished.
16. N. Nagaosa, “Quantum Field Theory in Strongly Correlated Electronic Systems”, (Springer, Berlin, 1999), Ch. 3.
17. P. Monthoux and D. Pines, *Phys. Rev.* **B47**, 6069 (1993); B.P. Stojković and D. Pines, *Phys. Rev.* **B55**, 8576 (1997).
18. A. Abanov, A.V. Chubukov, and J. Schmalian, cond-mat/0107421, to be published, *Adv. Phys.*
19. H.Q. Ding, *Phys. Rev. Lett.* **68**, 1927 (1992).
20. S. Chakravarty, B.I. Halperin, and D.R. Nelson, *Phys. Rev. Lett.* **60**, 1057 (1988).
21. F. Onufrieva, P. Pfeuty, and M. Kiselev, *Phys. Rev. Lett.* **82**, 2370 (1999); F. Onufrieva and P. Pfeuty, *Phys. Rev.* **B61**, 799 (2000).
22. J.C. Campuzano, H. Ding, M.R. Norman, H.M. Fretwell, M. Randeria, A. Kaminski, J. Mesot, T. Takeuchi, T. Sato, T. Yokoya, T. Takahashi, T. Mochiku, K. Kadowaki, P. Guptasarma, D.G. Hinks, Z. Konstantinovic, Z.Z. Li, and H. Raffy, *Phys. Rev. Lett.* **83**, 3709 (1999).
23. J.L. Tallon, J.R. Cooper, P.S.I.P.N. de Silva, G.V.M. Williams, and J.W. Loram, *Phys. Rev. Lett.* **75**, 4114 (1995).
24. N. Miyakawa, P. Guptasarma, J.F. Zasadzinski, D.G. Hinks, and K.E. Gray, *Phys. Rev. Lett.* **80**, 157 (1998).
25. N. Ichikawa, S. Uchida, J.M. Tranquada, T. Niemöller, P.M. Gehring, S.-H. Lee, and J.R. Schneider, *Phys. Rev. Lett.* **85**, 1738 (2000).
26. J.R. Schrieffer, X.G. Wen, and S.C. Zhang, *Phys. Rev.* **B39**, 11663 (1989).
27. J.M. Tranquada, B.J. Sternlieb, J.D. Axe, Y. Nakamura, and S. Uchida, *Nature* **375**, 561 (1995); J.M. Tranquada, J.D. Axe, N. Ichikawa, A.R. Moodenbaugh, Y. Nakamura, and S. Uchida, *Phys. Rev. Lett.* **78**, 338 (1997).
28. K.M. Lang, V. Madhavan, J.E. Hoffman, E.W. Hudson, H. Eisaki, S. Uchida, and J.C. Davis, *Nature* **415**, 412 (2002); S.H. Pan, J.P. O’Neal, R.L. Badzey, C. Chamon, H. Ding, J.R. Engelbrecht, Z. Wang, H. Eisaki, S. Uchida, A.K. Gupta, et. al., *Nature*; **413**, 282 (2001).
29. N. Harima, J. Matsuno, A. Fujimori, Y. Onose, Y. Taguchi, and Y. Tokura, cond-mat/0103519.
30. M. Ambai, Y. Kobayashi, S. Iikubo, and M. Sato, *J. Phys. Soc. Jpn.* **71**, 538 (2002).
31. R.S. Markiewicz, cond-mat/0108075, to be published as a Comment in *Phys. Rev. Lett.*
32. R.S. Markiewicz and C. Kusko, cond-mat/0102452, to be published, *Phys. Rev. B.*
33. E.J. Singley, D.N. Basov, K. Kurahashi, T. Uefuji, and K. Yamada, *Phys. Rev.* **B64**, 224503 (2001).
34. A. Singh, Z. Tešanović, H. Tang, G. Xiao, C.L. Chien, and J.C. Walker, *Phys. Rev. Lett.* **64**, 2571 (1990).
35. R.J. Birgeneau, H.J. Guggenheim, and G. Shirane, *Phys. Rev.* **B1**, 2211 (1970).